

## Accepted Manuscript

Title: Phase composition, microstructure and microwave dielectric properties of rock salt structured  $\text{Li}_2\text{ZrO}_3$ -MgO ceramics

Authors: J.X. Bi, C.F. Xing, C.H. Yang, H.T. Wu



PII: S0955-2219(18)30246-2  
DOI: <https://doi.org/10.1016/j.jeurceramsoc.2018.04.034>  
Reference: JECS 11844

To appear in: *Journal of the European Ceramic Society*

Received date: 29-9-2017  
Revised date: 14-4-2018  
Accepted date: 16-4-2018

Please cite this article as: Bi JX, Xing CF, Yang CH, Wu HT, Phase composition, microstructure and microwave dielectric properties of rock salt structured  $\text{Li}_2\text{ZrO}_3$ -MgO ceramics, *Journal of the European Ceramic Society* (2018), <https://doi.org/10.1016/j.jeurceramsoc.2018.04.034>

This is a PDF file of an unedited manuscript that has been accepted for publication. As a service to our customers we are providing this early version of the manuscript. The manuscript will undergo copyediting, typesetting, and review of the resulting proof before it is published in its final form. Please note that during the production process errors may be discovered which could affect the content, and all legal disclaimers that apply to the journal pertain.

Phase composition, microstructure and microwave dielectric properties of rock salt structured  $\text{Li}_2\text{ZrO}_3\text{-MgO}$  ceramics

J.X. Bi, C.F. Xing, C.H. Yang, H.T. Wu\*

School of Materials Science and Engineering, University of Jinan, Jinan 250022, China

\* Corresponding author.

Tel.: +86 531 82769782; fax: +86 531 87974453.

E-mail address: mse\_wuht@ujn.edu.cn (H.T. Wu).

1

## Abstract

A novel series of rock salt structured  $(1-x)\text{Li}_2\text{ZrO}_3\text{-}x\text{MgO}$  ceramics were prepared via the conventional solid state method. The tetragonal-cubic phase transition can be observed in the case of  $0.5 \leq x \leq 0.6$ , which has been testified by the results of XRD and SEM-EDS. Relatively dense and homogeneous microstructure can be obtained for all the compositions sintered at 1500 °C. With the x value increasing from 0.5 to 0.8, the relative permittivity linearly decreases from 16.50 to 12.65, and the  $\tau_f$  value decreases from  $\sim 10$  ppm/°C to  $\sim 35$  ppm/°C. The addition of MgO stabilizes the crystal structure and increases the bond energies in  $\text{Li}_2\text{ZrO}_3\text{-MgO}$  system, so there is an upward tendency in  $Q \cdot f$  values from  $\sim 77,000$  GHz to  $\sim 166,000$  GHz. Typically, the  $\text{Li}_2\text{Mg}_4\text{ZrO}_7$  ceramics sintered at 1500 °C possesses excellent properties with  $\epsilon_r=12.65$ ,  $Q \cdot f=165,924$  GHz and  $\tau_f=-34.66$  ppm/°C, which makes these materials good candidates for microwave devices.

**Keywords:** microwave dielectric properties;  $\text{Li}_2\text{ZrO}_3\text{-MgO}$  ceramics; bond energy; phase transition

## 1. Introduction

Low-permittivity microwave dielectric ceramics play an important role in a wide range of applications from millimeter wave communication to substrates for microwave integrated circuits, which promote the development of related industries such as Internet of Things (IoT), Direct-Broadcast Satellite (DBS), and Global Positioning System (GPS). To meet the demands for high-speed transmission, these materials should possess appropriate relative permittivities ( $\epsilon_r$ ), higher quality factors ( $Q \cdot f$ ) and near-zero temperature coefficients of resonant frequency ( $\tau_f$ ). In addition, lower sintering temperature and preparation costs are also required to make these materials suitable for practical applications [1, 2].

Recently, the rock salt structured  $\text{Li}_2\text{AO}_3\text{-MgO}$  (A=Ti, Zr, Sn) ternary system has attracted extensive attentions due to their excellent and adjustable microwave dielectric properties [3-16]. For instance, a series of  $(1-x)\text{Li}_2\text{TiO}_3\text{-}x\text{MgO}$  ceramics were synthesized according to the partial subsolidus phase diagram reported by A.R. West [3-11]. Although the relative

---

\* Corresponding author.

Tel.: +86 531 82769782; fax: +86 531 87974453.

E-mail address: mse\_wuht@ujn.edu.cn (H.T. Wu).

1

permittivity showed a downward tendency, the  $Q \cdot f$  values were considerably improved by an increasing amount of MgO addition. As a result, some typical compounds such as  $\text{Li}_2\text{MgTiO}_4$  ( $\epsilon_r=17.25$ ,  $Q \cdot f=97,300$  GHz,  $\tau_f=-27.2$  ppm/ $^\circ\text{C}$ , at  $1360^\circ\text{C}$ ) [5] and  $\text{Li}_2\text{Mg}_4\text{TiO}_7$  ( $\epsilon_r=13.43$ ,  $Q \cdot f=233,600$  GHz,  $\tau_f=-27.2$  ppm/ $^\circ\text{C}$ , at  $1600^\circ\text{C}$ ) [6] could be used for different industrial applications. Similar researches were also conducted in  $(1-x)\text{Li}_2\text{SnO}_3-x\text{MgO}$  system, and the  $\tau_f$  value could be shifted from positive to negative value at  $x=0.3$  [12-16]. However, there were fewer reports concerning about the phase formation and dielectric properties in  $(1-x)\text{Li}_2\text{ZrO}_3-x\text{MgO}$  ceramics.

The tetragonal  $\text{Li}_2\text{ZrO}_3$  ceramic, which possesses the space group of I41/amd, was reported to exhibit microwave dielectric properties with  $\epsilon_r=15.54$ ,  $Q \cdot f=37,166$  GHz,  $\tau_f=-26.60$  ppm/ $^\circ\text{C}$  [17]. On the other hand, the MgO ceramic belongs to the cubic system with the Fm-3m space group, which is well known as an ultra-low dielectric loss material in spite of the higher sintering temperature as well as the lower permittivity [18]. Since the cation size of  $\text{Mg}^{2+}$  (0.72 Å) is similar with that of  $\text{Zr}^{4+}$  (0.72 Å) and  $\text{Li}^+$  (0.76 Å) at the coordination number of 6,  $\text{Li}_2\text{ZrO}_3\text{-MgO}$  solid solutions can be achieved by ionic substitution [12, 13, 19, 20]. For example, the cubic structured  $\text{Li}_2\text{Mg}_3\text{ZrO}_6$  ceramics, which could be divided into  $0.25\text{Li}_2\text{ZrO}_3+0.75\text{MgO}$ , were reported to possess excellent dielectric properties of  $\epsilon_r=12.17$ ,  $Q \cdot f=113,000$  GHz, and  $\tau_f=-17.13$  ppm/ $^\circ\text{C}$  [12, 13]. In our previous work, the  $\text{Li}_2\text{MgZrO}_4$  ( $0.5\text{Li}_2\text{ZrO}_3-0.5\text{MgO}$ ) ceramic was found to possess tetragonal structure. Although the sample showed lower relative density (79.02%) at  $1175^\circ\text{C}$ , it exhibited suitable properties with  $\epsilon_r=12.30$ ,  $Q \cdot f=40,900$  GHz and  $\tau_f=-12.31$  ppm/ $^\circ\text{C}$  [20]. Thus, a tetragonal-cubic phase transition can be found in  $(1-x)\text{Li}_2\text{ZrO}_3-x\text{MgO}$  system and the  $x=0.50-0.75$  compositions are expected to exhibit mixed phases. In this work, the effects of intrinsic factors and extrinsic factors on the microwave dielectric properties of  $(1-x)\text{Li}_2\text{ZrO}_3-x\text{MgO}$  ceramics were systematically investigated. An appropriate  $\text{Li}_2\text{ZrO}_3\text{-MgO}$  ratio is expected to achieve balanced properties for practical applications.

## 2. Experimental procedure

The  $(1-x)\text{Li}_2\text{ZrO}_3-x\text{MgO}$  ( $x=0.5, 0.6, 0.7, 0.75$  and  $0.8$ ) ceramics were prepared via the conventional solid-state method and sintered by the atmosphere-protective method. Analytical-grade  $\text{Li}_2\text{CO}_3$ , MgO, and  $\text{ZrO}_2$  (Aladdin Shanghai Biochemical Technology Co., Ltd. Shanghai, China) were used as starting materials and mixed according to the pseudo phase diagram shown in Fig. 1. When  $x$  values were 0.5, 0.6, 0.7, 0.75 and 0.8, the chemical formula were  $\text{Li}_2\text{MgZrO}_4$ ,  $\text{Li}_4\text{Mg}_3\text{Zr}_2\text{O}_9$ ,  $\text{Li}_6\text{Mg}_7\text{Zr}_3\text{O}_{16}$ ,  $\text{Li}_2\text{Mg}_3\text{ZrO}_6$ ,  $\text{Li}_2\text{Mg}_4\text{ZrO}_7$ , respectively. At the first stage, the starting powders were milled for 24 h with anhydrous ethanol, dried and calcined at  $1050^\circ\text{C}$  for 2 h in alumina crucibles. The calcined powders were ground for another 24 h, dried and mixed with 8 wt% polyvinyl alcohol for granulation. Thereafter, the granulated powders were

pressed into pellets of 10 mm diameter and 6 mm height at a pressure of 200 MPa. Finally, these compacted pellets were preheated at 500 °C for 4 h to expel the binder, buried with sacrificial powders (Calcined powders with the same chemical composition of samples) and sintered at 1250-1550 °C for 6 h in platinum crucibles.

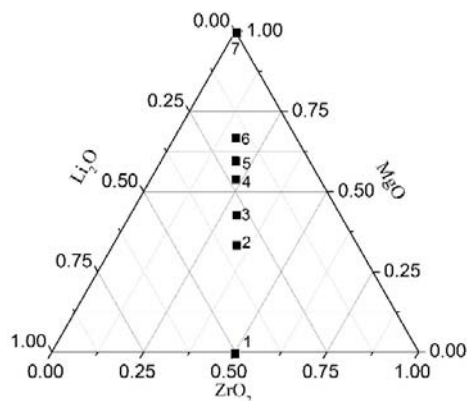


**Fig. 1** Pseudo phase diagram of the Li-Mg-Zr-O system (1~ $\text{Li}_2\text{ZrO}_3$ <sup>[17]</sup>, 2~ $\text{Li}_2\text{MgZrO}_4$ <sup>[20]</sup>, 3~ $\text{Li}_4\text{Mg}_3\text{Zr}_2\text{O}_9$ , 4~ $\text{Li}_6\text{Mg}_7\text{Zr}_3\text{O}_{16}$ , 5~ $\text{Li}_2\text{Mg}_3\text{ZrO}_6$ <sup>[13]</sup>, 6~ $\text{Li}_2\text{Mg}_4\text{ZrO}_7$  and 7~ $\text{MgO}$ <sup>[18]</sup>)

The apparent density of the sintered samples was measured using the Archimedes method (XS64, Mettler Toledo, USA). The crystal structure of  $(1-x)\text{Li}_2\text{ZrO}_3-x\text{MgO}$  was examined by an X-ray diffractometer (Model D/MAX-B, Rigaku Co., Japan). The surface morphology was characterized by a field-emission-scanning electron microscope (FeSEM Quanta 250, FEI Co., USA) coupled with energy dispersive X-ray spectroscopy (EDS). A network analyzer (N5234A, Agilent Co., America) was used for measuring microwave dielectric properties. The relative permittivity was measured using Hakki-Coleman post-resonator method by exciting the TE<sub>011</sub> resonant mode of dielectric resonator by using an electric probe as suggested by Hakki and Coleman [21]. The unloaded quality factor was measured using TE<sub>01d</sub> mode by the cavity method [22]. The corresponding temperature coefficient of resonant frequency of the samples was measured in the temperature range of 25-85 °C.

### 3. Results and discussion

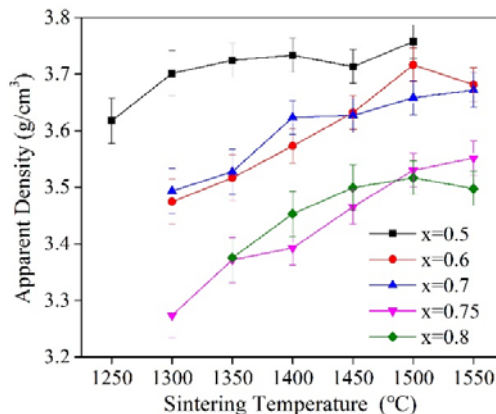


**Fig. 2** Apparent density of the  $(1-x)\text{Li}_2\text{ZrO}_3-x\text{MgO}$  ceramics sintered at 1250-1550 °C

Fig. 2 illustrates the apparent density of  $(1-x)\text{Li}_2\text{ZrO}_3-x\text{MgO}$  ceramics sintered at different temperatures. The addition of MgO can hinder the sintering process, because the low MgO content ceramics can obtain their maximum density at lower sintering temperature. All the samples possess saturated densities at 1500 °C, and they decrease from 3.76 g/cm<sup>3</sup> to 3.52 g/cm<sup>3</sup> as the x value increases from 0.5 to 0.8, implying the strong relevance between sintering characteristic and chemical composition. Although the atmosphere-protective method has been used in current work, the evaporation of lithium might still result in the weight loss and non-stoichiometric ratio at higher sintering temperatures, which has been testified by the weight loss of  $\text{Li}_2\text{Mg}_4\text{ZrO}_7$  ( $x=0.8$ ) ceramics shown in Fig. S1.

The X-ray powder diffraction (XRD) patterns of  $(1-x)\text{Li}_2\text{ZrO}_3-x\text{MgO}$  ceramics sintered at 1500 °C are shown in Fig. 3(a), and those of  $\text{Li}_2\text{MgZrO}_4$  ( $x=0.5$ ) and  $\text{Li}_6\text{Mg}_7\text{Zr}_3\text{O}_{16}$  ( $x=0.7$ ) ceramics sintered at different temperatures can be observed in Fig. S2. The primary phase is indexed as  $\text{Li}_2\text{MgZrO}_4$  with a tetragonal structure (I41/amd, PDF#36-0308) at  $x=0.5$  and  $x=0.6$ , while there are some small peaks associated the cubic-structured second phase (Fm-3m, PDF#45-0946). According to our previous report, pure  $\text{Li}_2\text{MgZrO}_4$  phase could be observed below 1175 °C when the ceramics were sintered for 4 h in air ambience, and the appearance of  $\text{ZrO}_2$  (monoclinic structure) was attributed to the evaporation of lithium at higher temperature [20]. However, the XRD result in this work unambiguously demonstrates the existence of cubic phase and the absence of  $\text{ZrO}_2$ . Hence, the different sintering processes and platinum crucibles can influence the formation of cubic phase to some extent, and the pure tetragonal phase is expected to exist in the case of  $x < 0.5$ . With the x value increasing from 0.5 to 0.6, the intensities of tetragonal phase get weakened and those of cubic phase get enhanced, which reflects that the latter phase has taken the large proportion in the  $\text{Li}_4\text{Mg}_3\text{Zr}_2\text{O}_9$  ( $x=0.6$ ) ceramics. All peaks are indexed as MgO (Fm-3m, PDF#45-0946) when x is higher than 0.7, implying that the cubic-structured solid solutions can be formed with an appropriate  $\text{Li}_2\text{ZrO}_3$ -MgO ratio. According the result shown in Fig. S2, there are no significant changes

on the XRD patterns for  $x=0.5$  &  $0.7$  ceramics sintered at different temperatures. Therefore,  $\text{Li}_2\text{ZrO}_3$ - $\text{MgO}$  ratio plays a more important role than sintering temperature on the phase composition within the region of  $1300$ - $1500$  °C.

Based on the above results, Rietveld refinement is performed by using FullProf suite, and  $\text{Li}_2\text{MgZrO}_4$  and  $\text{MgO}$  are chosen as starting models. The final refined plots, coupled with the crystallographic data for all samples sintered at  $1500$  °C are shown in Fig. S3 (a-e) and Table 1, respectively. With  $x$  value increasing from  $0.5$  to  $0.6$ , the relative content of tetragonal phase decreases from  $94.34\%$  to  $74.95\%$ , and that of cubic phase shows an upward tendency until the ceramic is completely full of cubic phase as  $x \geq 0.7$ . The variation in the unit cell volume of  $(1-x)\text{Li}_2\text{ZrO}_3$ - $x\text{MgO}$  ceramics is plotted in Fig. 3(b). Since the ionic size of  $\text{Mg}^{2+}$  ( $0.72$  Å) is smaller than that of  $\text{Li}^+$  ( $0.76$  Å) at a coordination number of  $6$ , the lattice parameters and cell volumes of  $(1-x)\text{Li}_2\text{ZrO}_3$ - $x\text{MgO}$  ( $0.7 \leq x \leq 0.8$ ) ceramics slightly decreases with the increasing  $\text{MgO}$  content. However, abnormal change is observed when  $x$  values increases from  $0.5$  to  $0.6$ , which should be investigated in future work because it might be associated with many factors such as phase composition, grain size, residual stress, ion valence state or defects.

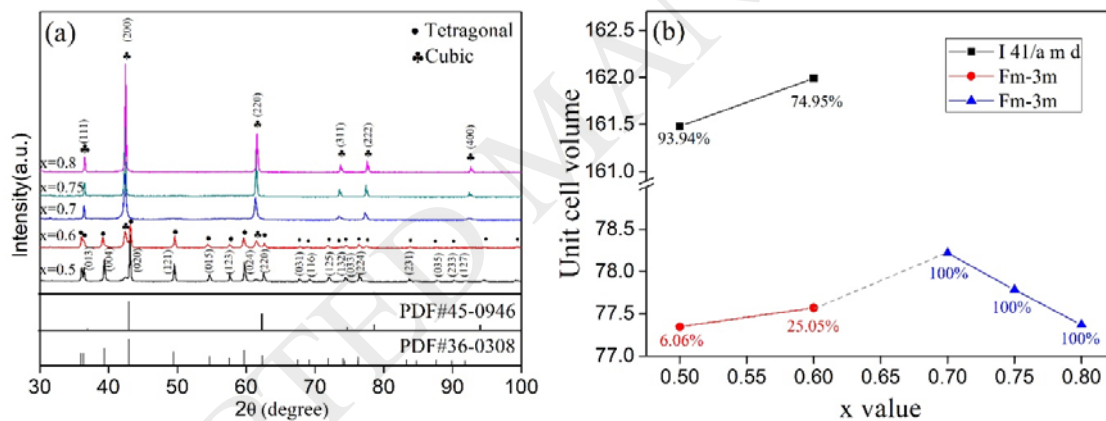


Fig. 3 (a) XRD patterns for the  $(1-x)\text{Li}_2\text{ZrO}_3$ - $x\text{MgO}$  ceramics sintered at  $1500$  °C (b) Variation of unit cell volume in  $(1-x)\text{Li}_2\text{ZrO}_3$ - $x\text{MgO}$  sintered at  $1500$  °C

Table 1 Molar content and refinement parameters of  $(1-x)\text{Li}_2\text{ZrO}_3$ - $x\text{MgO}$  ceramics sintered at  $1500$  °C

$x$	Space group	$n^a$	$\eta$ (%) <sup>b</sup>	$a=b$ (Å)	$c$ (Å)	$V$ (Å <sup>3</sup> )	$R_p$ (%)	$R_{wp}$ (%)
0.5	I 41/a m d	1	94.34	4.19858(2)	9.16027(3)	161.4779(21)	18.3	16.6
	Fm-3m	2/3	5.66	4.26071(1)	4.26071(1)	77.3474(5)		
0.6	I 41/a m d	1	74.95	4.19443(4)	9.20773(5)	161.9938(40)	15.8	16.9
	Fm-3m	2/3	25.05	4.26482(1)	4.26482(1)	77.5715(5)		
0.7	Fm-3m	1/4	100.00	4.27664(3)	4.27664(3)	78.2183(16)	14.0	16.9
0.75	Fm-3m	2/3	100.00	4.26866(4)	4.26866(4)	77.7812(22)	15.6	11.2
0.8	Fm-3m	4/7	100.00	4.26107(2)	4.26107(2)	77.3670(11)	19.0	14.3

<sup>a</sup> is the number of molecules in unit cell; <sup>b</sup>  $\eta$  is the phase content

According to the results of unit cell parameters listed in Table 1 and the apparent density shown in Table 2, the relative density of  $(1-x)\text{Li}_2\text{ZrO}_3-x\text{MgO}$  ( $0.7 \leq x \leq 0.8$ ) ceramics sintered at 1500 °C is calculated as Equ. 1 and Equ. 2.

$$\rho_{th} = \frac{nM}{NV} \quad (1)$$

$$\rho_{re} = \frac{\rho_{ap}}{\rho_{th}} \times 100\% \quad (2)$$

where  $n$  is the number of molecular in unit cell (see Table 1),  $M$  is the theoretical molecular weight,  $V$  is the refined unit cell volume (see Table 1) and  $N$  is Avogadro's number. As for  $x=0.5$  and  $x=0.6$ , the theoretic density of these mix-phase ceramics can be evaluated as follows.

$$\rho_{th} = \eta_1 \frac{n_1 M_1}{NV_1} + \eta_2 \frac{n_2 M_2}{NV_2} \quad (3)$$

where the subscripts of "1" and "2" indicate tetragonal and cubic phase,  $\eta$  is the phase content,  $M_1$  and  $M_2$  are temporarily defined as the molecular weights of  $\text{Li}_2\text{MgZrO}_4$  and  $\text{Li}_2\text{Mg}_3\text{ZrO}_6$ , respectively. As shown in Table 2, the relative density witnesses a downward tendency, decreasing from 94.5% to 90.5% as the  $x$  value increasing from 0.5 to 0.75, which indicates the relevance between sintering characteristics and MgO content. Considering the weight loss caused by evaporation of lithium at higher temperatures, the samples sintered at 1500 °C are considered as appropriate candidates for performing structure-property analysis.

**Table 2 Molecular volume, relative density, theoretical relative permittivity ( $\epsilon_{theo.}$ ), observed relative permittivity ( $\epsilon_r$ ) and porosity-corrected relative permittivity ( $\epsilon_{rc}$ ) of  $(1-x)\text{Li}_2\text{ZrO}_3-x\text{MgO}$  ceramics sintered at 1500 °C**

$x$	$V_m$ (Å <sup>3</sup> )	$\eta$ (%)	$\rho_{cal.}$ (g/cm <sup>3</sup> )	$\rho_{mea.}$ (g/cm <sup>3</sup> )	R.D. (%)	$\epsilon_r$	$\epsilon_{rc}$	$\epsilon_{theo.}$
0.5	161.4779(21)	94.34	3.98(0)	3.76(3)	94.5(7)	16.50(3)	17.84(3)	11.58(0)
	116.0212(8)	5.66						
0.6	161.9938(40)	74.95	3.95(0)	3.72(3)	94.2(7)	15.38(2)	16.75(2)	11.48(0)
	116.3572(8)	25.05						
0.7	312.8730(66)	100.00	3.94(0)	3.66(3)	92.9(8)	14.22(2)	15.73(2)	11.71(0)
0.75	116.6718(33)	100.00	3.90(0)	3.53(3)	90.5(8)	13.19(3)	15.14(3)	11.52(0)
0.8	135.3923(19)	100.00	3.86(0)	3.52(3)	91.2(8)	12.65(4)	14.34(5)	11.24(0)

Fig. 4 shows the backscattered electron images (BEI) of  $\text{Li}_2\text{MgZrO}_4$  ( $x=0.5$ ) and  $\text{Li}_4\text{Mg}_3\text{Zr}_2\text{O}_9$  ( $x=0.6$ ) ceramics sintered at 1500 °C. It can be observed that two types of grains co-exist in these ceramics, which agrees well with the XRD

result shown in Fig. 3(a). In order to clarify the phase compositions for both grains, EDS is conducted in  $\text{Li}_4\text{Mg}_3\text{Zr}_2\text{O}_9$  ceramic sintered at  $1500\text{ }^\circ\text{C}$ . Since the beryllium window tube of detector absorbs X-ray on lightweight elements, the Li element in the ceramics cannot be detected in this work. The granular crystals exhibit a Mg-rich phase with an element ratio of  $\text{Mg}:\text{Zr}:\text{O}=19.94:13.81:66.25$ , while those rod-like crystals exhibit a Zr-rich phase with a ratio of  $\text{Mg}:\text{Zr}:\text{O}=19.25:16.10:64.65$ , indicating that a mixture of cubic and tetragonal phase can be formed at  $x=0.6$ . Secondary electron images (SEI) of  $\text{Li}_6\text{Mg}_7\text{Zr}_3\text{O}_{16}$  ( $x=0.7$ ),  $\text{Li}_2\text{Mg}_3\text{ZrO}_6$  ( $x=0.75$ ) and  $\text{Li}_2\text{Mg}_4\text{ZrO}_7$  ( $x=0.8$ ) ceramics sintered at  $1500\text{ }^\circ\text{C}$  are shown in Fig. 5. All the samples exhibit dense microstructures with homogeneous grains, which is inconsistent with the relative density shown in Table 2. Since the oxide ceramics are poor conductors of heat, temperature gradient will appear in the sintering process. As a result, the surface of the sample possesses higher density than that in the interior of sample, which has been testified by the cross-sectional SEM micrographs shown in Fig. S4.

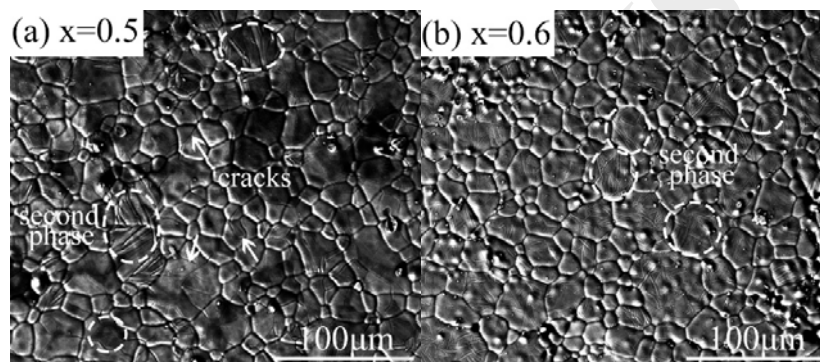


Fig. 4 Backscattered electron images (BEI) of (a)  $\text{Li}_2\text{MgZrO}_4$  ( $x=0.5$ ) and (b)  $\text{Li}_4\text{Mg}_3\text{Zr}_2\text{O}_9$  ( $x=0.6$ ) ceramics sintered at  $1500\text{ }^\circ\text{C}$

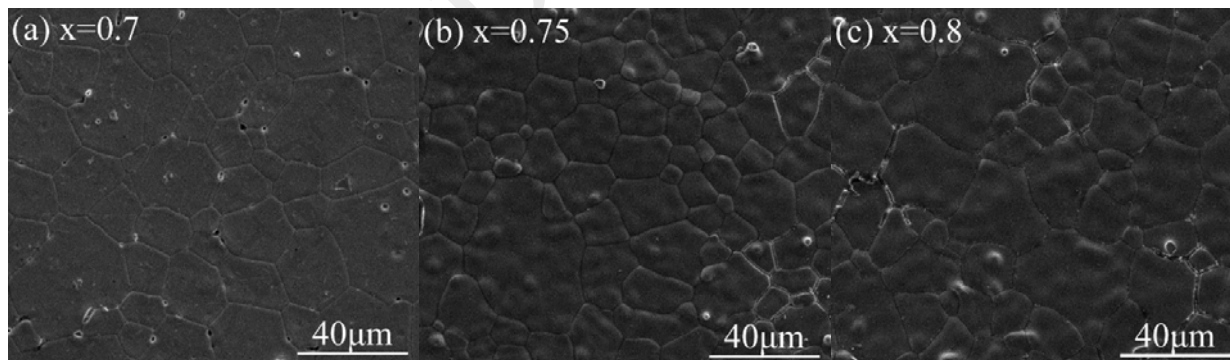


Fig. 5 Secondary electron images (SEI) of (a)  $\text{Li}_6\text{Mg}_7\text{Zr}_3\text{O}_{16}$  ( $x=0.7$ ), (b)  $\text{Li}_2\text{Mg}_3\text{ZrO}_6$  ( $x=0.75$ ) and (c)  $\text{Li}_2\text{Mg}_4\text{ZrO}_7$  ( $x=0.8$ ) ceramics sintered at  $1500\text{ }^\circ\text{C}$

The relative permittivity of  $(1-x)\text{Li}_2\text{ZrO}_3-x\text{MgO}$  ceramics sintered at different temperatures is shown in Fig. 6(a). The  $\epsilon_r$  values increase with the increasing relative densities (decreasing porosities) at lower sintering temperatures, while they depend more on intrinsic factors such as chemical composition and crystal structure when they densified at  $1500\text{ }^\circ\text{C}$ . In

order to investigate effects of crystal structure on the dielectric characteristic of  $(1-x)\text{Li}_2\text{ZrO}_3-x\text{MgO}$  ceramics, the Shannon's additive rule is used to calculate ionic polarizability ( $\alpha_{\text{theo.}}$ ).

$$\alpha_{\text{theo.}} = (2 - 2x)\alpha(\text{Li}^+) + x\alpha(\text{Mg}^{2+}) + (1 - x)\alpha(\text{Zr}^{4+}) + (3 - 2x)\alpha(\text{O}^{2-}) \quad (4)$$

where  $\alpha(\text{Li}^+)$ ,  $\alpha(\text{Mg}^{2+})$ ,  $\alpha(\text{Zr}^{4+})$  and  $\alpha(\text{O}^{2-})$  are the ions polarizabilities reported in Shannon's literature [23]. Thereafter, the theoretical relative permittivities are calculated by Clausius-Mossotti equation shown in Equ. 5 [24].

$$\epsilon_{\text{theo.}} = \frac{3V_m + 8\pi\alpha_{\text{theo.}}}{3V_m - 4\pi\alpha_{\text{theo.}}} \quad (5)$$

where  $V_m$  is the calculated molar volume (see Table 2). Since there are two phases distributing in the  $\text{Li}_2\text{MgZrO}_4$  and  $\text{Li}_4\text{Mg}_3\text{Zr}_2\text{O}_9$  composite ceramics, the corresponding relative permittivities should be calculated by Lichtenecker logarithmic rule [25].

$$\epsilon_{\text{theo.}} = v_1 \ln(\epsilon_1) + v_2 \ln(\epsilon_2) \quad (6)$$

where  $v_1$  and  $v_2$  represent the volume fractions of tetragonal and cubic phases.  $\alpha(\text{Li}_2\text{MgZrO}_4)$  and  $\alpha(\text{Li}_4\text{Mg}_3\text{Zr}_2\text{O}_9)$  are temporarily used to define the theoretical ionic polarizabilities in composite materials. For the samples sintered at 1500 °C, porosity-corrected permittivity ( $\epsilon_{rc}$ ) is calculated to eliminate the influence of porosity on the observed  $\epsilon_r$  values.

$$\frac{\epsilon_{\text{obs.}} - \epsilon_{rc}}{3\epsilon_{\text{obs.}}} = \frac{\delta(\epsilon_1 - \epsilon_{rc})}{\epsilon_1 + 2\epsilon_{\text{obs.}}} \quad (7)$$

where  $\epsilon_r$  is the observed relative permittivity,  $\epsilon_1$  is permittivity of porosity (defined as 1),  $\delta$  was the fractional porosity.

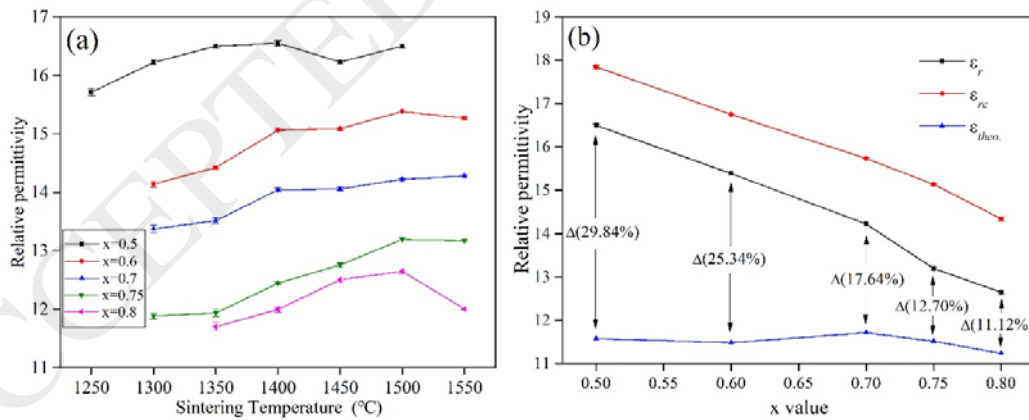


**Fig. 6** Relative permittivity of  $(1-x)\text{Li}_2\text{ZrO}_3-x\text{MgO}$  ceramics as a function of sintering temperature (b) Variation of theoretical relative permittivity ( $\epsilon_{\text{theo.}}$ ), observed relative permittivity ( $\epsilon_r$ ) and porosity-corrected relative permittivity ( $\epsilon_{rc}$ ) of  $(1-x)\text{Li}_2\text{ZrO}_3-x\text{MgO}$  ceramics sintered at 1500 °C

The theoretical relative permittivity ( $\epsilon_{\text{theo.}}$ ), observed relative permittivity ( $\epsilon_r$ ) and porosity-corrected relative permittivity ( $\epsilon_{rc}$ ) of  $(1-x)\text{Li}_2\text{ZrO}_3-x\text{MgO}$  ceramics sintered at 1500 °C are listed in Table 2, and the relationship between

dielectric permittivity and  $\text{Li}_2\text{ZrO}_3\text{-MgO}$  ratio is illustrated in Fig. 6(b). With the  $x$  value increasing from 0.5 to 0.8, the  $\epsilon_{rc}$  values linearly decreases from 17.84 to 14.34, and these values are slightly higher than the measured values (12.65-16.50), implying that the dielectric characteristic is mainly dependent on intrinsic and structural factors. However, there is a significant discrepancy between  $\epsilon_{theo.}$  and  $\epsilon_r$  values with a deviation ( $\Delta$ ) more than 10%, which indicates that the peculiar crystal chemistry of  $(1-x)\text{Li}_2\text{ZrO}_3\text{-xMgO}$  ceramics might enhance the relative permittivity beyond the value expected from the Clausius-Mossotti equation. Similar results can be also observed in  $\text{Li}_2\text{Mg}_3\text{BO}_6$  (B=Ti, Sn, Zr) system reported in previous works, and “structural change” such as local atomic motion or polyhedral distortion is considered the reason for above deviations [12, 13, 23]. Indeed, the gap between  $\epsilon_{theo.}$  and  $\epsilon_r$  values gradually decreases from 29.84% to 11.12% with the increasing  $x$  value. Since both the  $\text{LiO}_6$  and  $(\text{Mg,Zr})\text{O}_6$  octahedra are distorted in tetragonal phase, the cation and anion are more likely to move to adjust configuration at high frequencies, which might increase the relative permittivity of  $\text{Li}_2\text{MgZrO}_4$  and  $\text{Li}_4\text{Mg}_3\text{Zr}_2\text{O}_9$  ceramics [26]. When the tetragonal phase has been transformed into cubic phase, “structural changes” becomes less significant, and there might be less “rattling” or “compressed” cations with the increasing MgO content.

Fig. 7(a) demonstrates the  $Q:f$  values of  $(1-x)\text{Li}_2\text{ZrO}_3\text{-xMgO}$  ceramics sintered at different temperatures. In general, several factors lead to the dielectric loss in the microwave range and these factors can be divided into two parts: intrinsic loss and extrinsic loss [2, 27]. In this work, the extrinsic losses are caused by porosity, second phases, defects or microcracks, while the phase composition or internal vibrations will be contributed to the intrinsic loss. As shown in Fig. 7(a), all curves of  $Q:f$  values exhibit similar trends with those of apparent densities, which indicates the strong relevance between porosity and dielectric loss at lower temperature. It is worth mentioning that both the  $\text{Li}_2\text{MgZrO}_4$  and  $\text{Li}_4\text{Mg}_3\text{Zr}_2\text{O}_9$  ceramics possess multiphase, and some microcracks can be observed on the surface of  $\text{Li}_2\text{MgZrO}_4$  sintered at 1500 °C. Therefore, it is difficult to determine the contribution of different types of loss mechanisms to  $Q:f$  values under the above situation. Once the  $x$  value is higher than 0.7, the difference between  $Q:f$  values for ceramics sintered at 1500 °C is mainly caused by varied intrinsic factors, because they possess single phase as well as similar lower porosities. It is reported that higher bond energy can stabilize the crystal structure and the  $Q:f$  values might be predicted by the variation of bond energy [28, 29]. According to the chemical bond and the electronegativity theory, the individual bond energy in cubic-structured ceramics is calculated and divided into ionicity part and covalence part [30-32].

$$E_b^\mu = t_c E_c^\mu + t_i E_i^\mu \quad (8)$$

$$E_c^\mu = \frac{(r_{cA} + r_{cB})}{d^\mu} (E_{A-A} E_{B-B})^{1/2} (\text{KJ} / \text{mol}) \quad (9)$$

$$E_i^\mu = \frac{1389.088}{d^\mu} (\text{KJ} / \text{mol}) \quad (10)$$

where  $r_{cA}$  and  $r_{cB}$  are the covalent radii,  $E_{A-A}$  and  $E_{B-B}$  are the homonuclear bond energy obtained from the handbook of bond energies [33]. As for  $t_c$  and  $t_i$ , these values are defined as covalent and ionic proportional coefficient in individual bond and calculated as following equations.

$$t_c + t_i = 1 \quad (11)$$

$$t_i = \left| \frac{(S_A - S_B)}{6} \right| \quad (12)$$

where  $S_A$  and  $S_B$  are the electronegativities of A and B ions. The calculated results are listed in Table S1 and the correlation among Li-O, Zr-O, Mg-O bond energies and  $Q \cdot f$  values of  $(1-x)\text{Li}_2\text{ZrO}_3-x\text{MgO}$  ceramics is demonstrated in Fig. 7(b). As shown in Table S1, the Zr-O bond has the largest covalent bond energy, with about 390 KJ/mol, followed by Ti-O bond (about 210 KJ/mol), while the energy in Li-O bond is the lowest, with only about 71 KJ/mol. Since all types of bonds possess same length, there is no change in the ionicity energies at the specified chemical composition. With the  $x$  value increasing from 0.7 to 0.8, the bond length in  $(1-x)\text{Li}_2\text{ZrO}_3-x\text{MgO}$  ceramics gradually decreases from 2.1383 Å to 2.1306 Å, resulting in an upward tendency of bond energy in all typical bonds. Thus, it can be speculated that the addition of MgO increases the stability of individual bonds and decreases the dielectric losses in cubic structured  $(1-x)\text{Li}_2\text{ZrO}_3-x\text{MgO}$  ceramics.

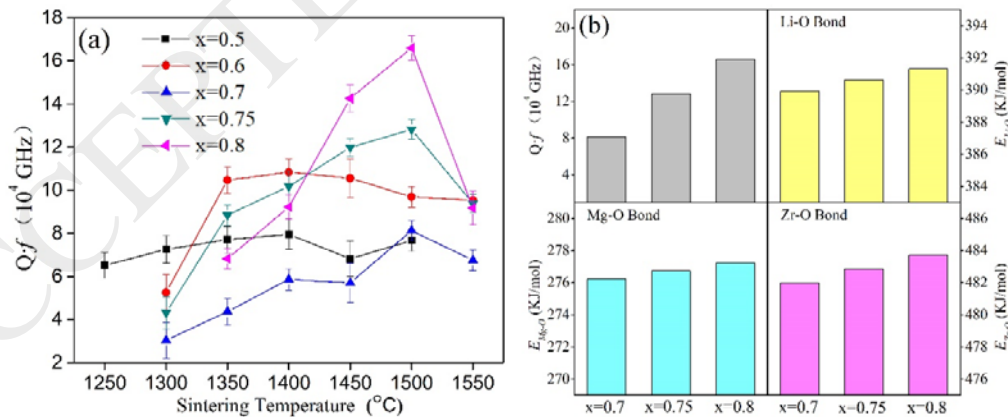


**Fig. 7 (a)  $Q \cdot f$  values of  $(1-x)\text{Li}_2\text{ZrO}_3-x\text{MgO}$  ceramics as a function of sintering temperature (b) Relationship among Li-O, Zr-O, Mg-O bond energies and  $Q \cdot f$  values of  $\text{Li}_6\text{Mg}_7\text{Zr}_3\text{O}_{16}$  ( $x=0.7$ ),  $\text{Li}_2\text{Mg}_3\text{ZrO}_6$  ( $x=0.75$ ) and  $\text{Li}_2\text{Mg}_4\text{ZrO}_7$  ( $x=0.8$ ) ceramics sintered at 1500 °C**

Fig. 8 discusses the correlation between MgO content and temperature coefficients of resonant frequency ( $\tau_f$ ) of  $(1-x)\text{Li}_2\text{ZrO}_3-x\text{MgO}$  ceramics sintered at 1500 °C. The  $\tau_f$  value is defined as the combination of coefficient of dielectric

constant ( $\tau_e$ ) and the thermal expansion coefficient ( $\alpha$ ), while the latter can be neglected due to their lower coefficient ( $|\alpha| < 10 \text{ ppm}/^\circ\text{C}$ ) [34]. As shown in Fig. 8, the  $\tau_f$  value linearly decreases from  $-21.96 \text{ ppm}/^\circ\text{C}$  at  $x=0.7$  to  $-34.66 \text{ ppm}/^\circ\text{C}$  at  $x=0.8$ . According to the data obtained from the handbook of bond energies, a sequence of the dissociation energies of  $E_{\text{Mg-Mg}}(11.3\text{kJ/mol}) < E_{\text{Li-Li}}(105.0\text{kJ/mol}) < E_{\text{Zr-Zr}}(298.2\text{kJ/mol})$  can be identified. Thus, in spite of the increasing individual bond energy shown in Table S1, the addition of MgO significantly decreases the total bond energies of unit cell and influences the  $\tau_f$  values in cubic-structured  $\text{Li}_2\text{ZrO}_3$ -MgO ceramics. The  $\tau_f$  value of  $\text{Li}_4\text{Mg}_3\text{Zr}_2\text{O}_9$  ( $x=0.6$ ) is slightly lower than that of  $\text{Li}_6\text{Mg}_7\text{Zr}_3\text{O}_{16}$  ( $x=0.7$ ), which indicates that the phase composition plays a certain role in affecting the temperature stability of the ceramics. The above explanation needs to be further discussed by more precise experiments, which are beyond the study in this work.

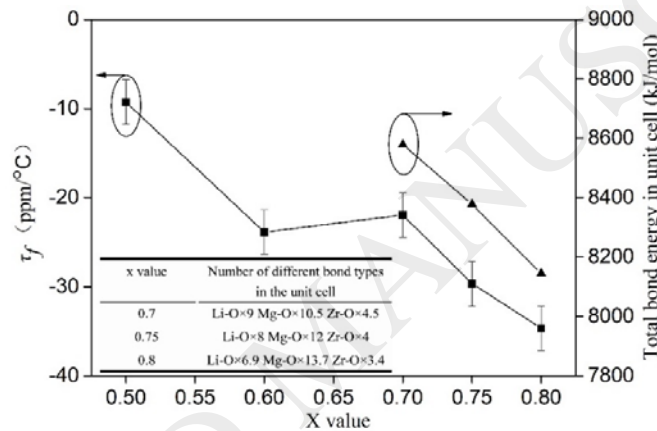


**Fig. 8 Temperature coefficients of resonant frequency ( $\tau_f$ ) of  $(1-x)\text{Li}_2\text{ZrO}_3$ - $x\text{MgO}$  ceramics sintered at  $1500^\circ\text{C}$  and corresponding total bond energy in unit cell**

#### 4. Conclusion

$(1-x)\text{Li}_2\text{ZrO}_3$ - $x\text{MgO}$  ( $x=0.5, 0.6, 0.7, 0.75$  and  $0.8$ ) ceramics were successfully prepared by the conventional solid-state method. The XRD and EDS analysis demonstrates that multiphase can co-exist in the  $x=0.5$ - $0.6$  composition, and single phase with cubic structure appears in the case of  $x>0.7$ . Changes in the microwave dielectric properties are caused by the transformation of the microstructure as a crucial intrinsic factor. The lower polarizability of  $\text{Mg}^{2+}$  in comparison with  $\text{Zr}^{4+}$  results in the decrease in relative permittivity, while the local atomic motion or polyhedral distortion might cause a significant deviation between  $\epsilon_{theo.}$  and  $\epsilon_r$  values. The changed crystal structure can be explained by the variation of individual bond energy, which plays a major role in affecting the  $Q \cdot f$  value. Although the addition of MgO enhances stability of individual bond, the downward tendency in the total bond energies of unit cell is considered as a main factor in the decrease of the  $\tau_f$  values. In addition, the microwave dielectric properties are also affected by extrinsic factors such as

apparent density, second phases and microcracks. All the ceramics possess more than 90% theoretical density at 1500 °C with excellent microwave dielectric properties of  $\epsilon_r \sim 12.5-16.5$ ,  $Q \cdot f \sim 77,000-166,000$  GHz and  $\tau_f \sim -10$  ppm/°C to  $-35$  ppm/°C. In addition, a good combination of properties can be found in  $\text{Li}_2\text{Mg}_4\text{ZrO}_7$  ceramics sintered at 1500 °C ( $\epsilon_r = 12.65$ ,  $Q \cdot f = 165,924$  GHz and  $\tau_f = -34.66$  ppm/°C), indicating that the system is a suitable candidate for further investigation or industrial applications.

### Acknowledgments

This work was supported by the National Natural Science Foundation (No. 51472108) and Project funded by China Postdoctoral Science Foundation (2017M612341). The authors are thankful to the help of Professor Zhenxing Yue and postdoctoral Jie Zhang on the measurement of microwave dielectric properties in Tsinghua University.

### Reference

- [1] M.T. Sebastian, Dielectric materials for wireless communication, Elsevier, Oxford, 2008.
- [2] M.T. Sebastian, R. Uvic, H. Jantunen, Low-loss dielectric ceramic materials and their properties, *Int. Mater. Rev.* 60 (2015) 392-412.
- [3] M. Castellanos, A.R. West, Order-disorder phenomena in oxides with rock salt structures: the system  $\text{Li}_2\text{TiO}_3\text{-MgO}$ , *J. Mater. Sci.* 14 (1979) 450-454.
- [4] J.J. Bian, Y.F. Dong, New high Q microwave dielectric ceramics with rock salt structures:  $(1-x)\text{Li}_2\text{TiO}_3\text{-xMgO}$  system ( $0 \leq x \leq 0.5$ ), *J. Eur. Ceram. Soc.* 2 (2010) 325-330.
- [5] Y.W. Tseng, J.Y. Chen, Y.C. Kuo, C.L. Huang, Low-loss microwave dielectrics using rock salt oxide  $\text{Li}_2\text{MgTiO}_4$ , *J. Alloys Compd.* 509 (2015) L308-L310.
- [6] J.X. Bi, C.C. Li, Y.H. Zhang, C.F. Xing, C.H. Yang, H.T. Wu, Crystal structure, infrared spectra and microwave dielectric properties of novel  $\text{Li}_2\text{Mg}_4\text{TiO}_7$  ceramics, *Mater. Lett.* 196 (2017) 128-131.
- [7] H.F. Zhou, X.H. Tan, J. Huang, N. Wang, G.H. Fan, X.L. Chen, Phase structure, sintering behavior and adjustable microwave dielectric properties of  $\text{Mg}_{1-x}\text{Li}_{2x}\text{Ti}_x\text{O}_{1+2x}$  solid solution ceramics, *J. Alloys Compd.* 696 (2017) 1255-1259.
- [8] H.F. Zhou, X.H. Tan, J. Huang, X.L. Chen, Sintering behavior, phase evolution and microwave dielectric properties of thermally stable  $\text{Li}_2\text{O-3MgO-mTiO}_2$  ceramics ( $1 \leq m \leq 6$ ), *Ceram. Int.* 43 (2017) 3688-3692.

- [9] Y.D. Zhang, D. Zhou, Pseudo phase diagram and microwave dielectric properties of  $\text{Li}_2\text{O-MgO-TiO}_2$  ternary system, *J. Am. Ceram. Soc.* 99 (2016) 3645-3650.
- [10] J.X. Bi, Y.J. Niu, H.T. Wu,  $\text{Li}_4\text{Mg}_3\text{Ti}_2\text{O}_9$ : A novel low-loss microwave dielectric ceramic for LTCC applications, *Ceram. Int.* 43 (2017) 7522-7530.
- [11] H.L. Pan, H.T. Wu, Crystal structure, infrared spectra and microwave dielectric properties of new ultra low-loss  $\text{Li}_6\text{Mg}_7\text{Ti}_3\text{O}_{16}$  ceramics, *Ceram. Int.* 43 (2017) 14484-14487.
- [12] Z.F. Fu, P. Liu, J.L. Ma, X.G. Zhao, H.W. Zhang, Novel series of ultra-low loss microwave dielectric ceramics:  $\text{Li}_2\text{Mg}_3\text{BO}_6$  (B = Ti, Sn, Zr), *J. Eur. Ceram. Soc.* 3 (2016) 625-629.
- [13] H.T. Wu, E.S. Kim, Correlations between crystal structure and dielectric properties of high-Q materials in rock-salt structure  $\text{Li}_2\text{O-MgO-BO}_2$  (B=Ti, Sn, Zr) systems at microwave frequency, *RSC Adv.* 6 (2016) 47443-47453.
- [14] C.W. Liu, N.X. Wu, Y.L. Mao, J.J. Bian, Phase formation, microstructure and microwave dielectric properties of  $\text{Li}_2\text{SnO}_3\text{-MO}$  (M=Mg, Zn) ceramics, *J. Electroceram.* 32 (2014) 199-204.
- [15] M. Castellanos, Compound and solid solution formation in the system,  $\text{Li}_2\text{SnO}_3\text{-MgO}$ , *J. Mater. Sci. Lett.* 3 (1984) 786-788.
- [16] Z.X. Fang, B. Tang, F. Si, E.Z. Li, H.Y. Yang, S.R. Zhang, Phase evolution, structure and microwave dielectric properties of  $\text{Li}_{2+x}\text{Mg}_3\text{SnO}_6$  ( $x=0.00\text{-}0.12$ ) ceramics, *Ceram. Int.* 43 (2017) 13645-13652.
- [17] L.L. Yuan, J.J. Bian, Microwave dielectric properties of the lithium containing compounds with rock salt structure, *Ferroelectrics* 387 (2009) 123-129.
- [18] A. Kan, T. Moriyama, S. Takahashi, H. Ogawa, Low-temperature sintering and microwave dielectric properties of MgO ceramic with LiF addition, *Jpn. J. Appl. Phys.* 50 (2011) 1489-1496.
- [19] J. Song, J. Zhang, R.Z. Zuo, Ultrahigh Q values and atmosphere-controlled sintering of  $\text{Li}_{2(1+x)}\text{Mg}_3\text{ZrO}_6$  microwave dielectric ceramics, *Ceram. Int.* 43 (2017) 2246-2251.
- [20] J.X. Bi, C.F. Xing, X.S. Jiang, C.H. Yang, H.T. Wu, Characterization and microwave dielectric properties of new low loss  $\text{Li}_2\text{MgZrO}_4$  ceramics, *Mater. Lett.* 184 (2016) 269-272.
- [21] B.W. Hakki, P.D. Coleman, A dielectric resonator method of measuring inductive capacities in the millimeter range, *IRE Trans. Microwave TheoryTech.* 8 (1960) 402-410.
- [22] W.E. Courtney, Analysis and evaluation of a method of measuring the complex permittivity and permeability of microwave insulators, *IEEE Trans. Microwave Theory Tech.* 18 (1970) 476-485.

- [23] R.D. Shannon, G.R. Rossman, Dielectric constants of silicate garnets and the oxide additivity rule, *Am. Miner.* 77 (1992) 94-100.
- [24] R.D. Shannon, Dielectric polarizabilities of ions in oxides and fluorides, *J. Appl. Phys.* 73 (1993) 348-366.
- [25] Y. Imanaka, Multilayered low temperature cofired ceramics (LTCC) technology, Springer-Verlag, New York, 2005.
- [26] J.D. Dunitz, L.E. Orgel, Stereochemistry of ionic solids, *Adv. Inorg. Chem. Radiochem.* 2 (1960) 1-60.
- [27] J. Zhang, Z.X. Yue, Y. Luo, X.H. Zhang, L.T. Li, Understanding the thermally stimulated relaxation and defect behavior of Ti-containing microwave dielectrics: A case study of BaTi<sub>4</sub>O<sub>9</sub>, *Mater. Design.* 130 (2017) 479-487.
- [28] E.S. Kim, B.S. Chun, R. Freer, R.J. Cernik, Effects of packing fraction and bond valence on microwave dielectric properties of A<sup>2+</sup>B<sup>6+</sup>O<sub>4</sub> (A<sup>2+</sup>: Ca, Pb, Ba; B<sup>6+</sup>: Mo, W) ceramics, *J. Eur. Ceram. Soc.* 30 (2010) 1731-1736.
- [29] S.H. Kim, E.S. Kim, Intrinsic factors affecting the microwave dielectric properties of Mg<sub>2</sub>Ti<sub>1-x</sub>(Mg<sub>1/3</sub>Sb<sub>2/3</sub>)<sub>x</sub>O<sub>4</sub> ceramics, *Ceram. Int.* 42 (2016) 15035-15040.
- [30] R.T. Sanderson, Multiple and single bond energies in inorganic molecules, *Inorg. Nucl. Chem.* 30 (1968) 375-393.
- [31] R.T. Sanderson, Chemical bonds, bond energy, Academic press, New York, 1971.
- [32] R.T. Sanderson, Electronegativity and bond energy, *J. Am. Chem. Soc.* 105 (1983) 2259-2261.
- [33] Y.R. Luo, Comprehensive handbook of chemical bond energies, CRC press, Boca Raton, 2007.
- [34] S.D. Ramarao, V.R.K. Murthy, Structural, Raman spectroscopic and microwave dielectric studies on Ni<sub>1-x</sub>(Zn<sub>1/2</sub>Zr<sub>1/2</sub>)<sub>x</sub>W<sub>1-x</sub>Nb<sub>x</sub>O<sub>4</sub> ceramic compounds with wolframite structure, *Dalton Trans.* 44 (2015) 2311-2324.